

Propagation of pacemaker activity

Ronald W. Joyner · Ronald Wilders ·
Mary B. Wagner

Received: 3 April 2006 / Accepted: 11 August 2006 / Published online: 2 September 2006
© International Federation for Medical and Biological Engineering 2006

Abstract Spontaneous activity of specific regions (e.g., the Sinoatrial node, SAN) is essential for the normal activation sequence of the heart and also serve as a primary means of modulating cardiac rate by sympathetic tone and circulating catecholamines. The mechanisms of how a small SAN region can electrically drive a much larger atrium, or how a small ectopic focus can drive surrounding ventricular or atrial tissue are complex, and involve the membrane properties and electrical coupling within the SAN or focus region as well as the membrane properties, coupling conductance magnitudes and also regional distribution within the surrounding tissue. We review here studies over the past few decades in which mathematical models and experimental studies have been used to determine some of the design principles of successful propagation from a pacemaking focus. These principles can be briefly summarized as (1) central relative uncoupling to protect the spontaneously firing cells from too much electrotonic inhibition, (2) a transitional region in which the cell type and electrical coupling change from the central SAN region to the peripheral atrial region, and (3) a distributed anisotropy to facilitate focal activity.

Keywords Sinoatrial node · Electrical coupling · Action potential propagation · Cardiac rhythm · Cardiac cell electrophysiology · Numerical simulations

1 Introduction

There are several regions of the heart in which spontaneous generation of action potentials can potentially occur. These include the normally dominant pacemaker region of the sinoatrial node but also regions such as the atrioventricular node and the Purkinje system whose intrinsic automaticity is normally suppressed by the faster automaticity of the sinoatrial node area. In addition, other regions of the heart may, under pathological conditions, also demonstrate automaticity which may lead to single ectopic beats, initiation of reentrant tachycardia, or persistent focal tachycardia [1, 11]. One common feature of both normal and abnormal manifestations of automaticity is the propagation of the action potential from the automatic region to the quiescent surrounding atrial or ventricular tissue. While the presence of a coupling conductance between the automatic focus and the surrounding cells is necessary for propagation out from the focus region, this coupling conductance may also suppress the activity of the focus region by electrotonic interactions during the diastolic depolarization phase of the focus cells. This loading effect depends on many factors, including the size (number of cells) of the focus region, the intercellular coupling among the focus cells, the input resistance of the surrounding quiescent cells, and the value and spatial orientation of the coupling conductances among the surrounding cells. Another factor that is less well appreciated is that the focus

R. W. Joyner (✉) · M. B. Wagner
Department of Pediatrics, Emory University
School of Medicine, 2015 Uppergate Drive NE,
Atlanta, GA 30322, USA
e-mail: rjoyner@cellbio.emory.edu

R. Wilders
Department of Physiology, Academic Medical Center,
Amsterdam, The Netherlands

region itself may be inhomogeneous both in terms of membrane properties as well as in the distribution of cellular coupling [7, 8]. In this review, we will illustrate some of the experimental and theoretical studies, which have been done to determine some of the interactions among these factors.

2 Interactions among spontaneously pacing cells

When cells with intrinsically different spontaneously pacing rates are electrically connected, they might be expected to in some way “synchronize” their pacing to form a better current source for activation of surrounding quiescent tissue. A number of simulation and experimental studies have been done on this phenomenon. We did some early simulations [13] with the Noma–Irisawa [10] model of spontaneously pacing SA

nodal cells in which we assumed two populations of cells: one with the normal model properties and another group with increased L -type calcium current ($2 \times I_{si}$) such that their automaticity was increased. In this case we considered these to be two aggregates of cells (similar to the chick embryo cell aggregates experimentally studied later on by Veenstra and DeHaan [19]) with each model aggregate having a membrane area of 1 mm^2 . As shown in Fig. 1 the resulting cycle length (CL) for low coupling resistance is the same as if there were a single aggregate with an average value of 1.5 times the normal I_{si} . However, as the coupling resistance between the aggregates was increased, the synchronized CL increased toward the value of the faster aggregate. As the synchronized CL increased there was also a greater delay between the activation times of the two aggregates and a greater disparity in the maximum dV/dt of the upstrokes of the

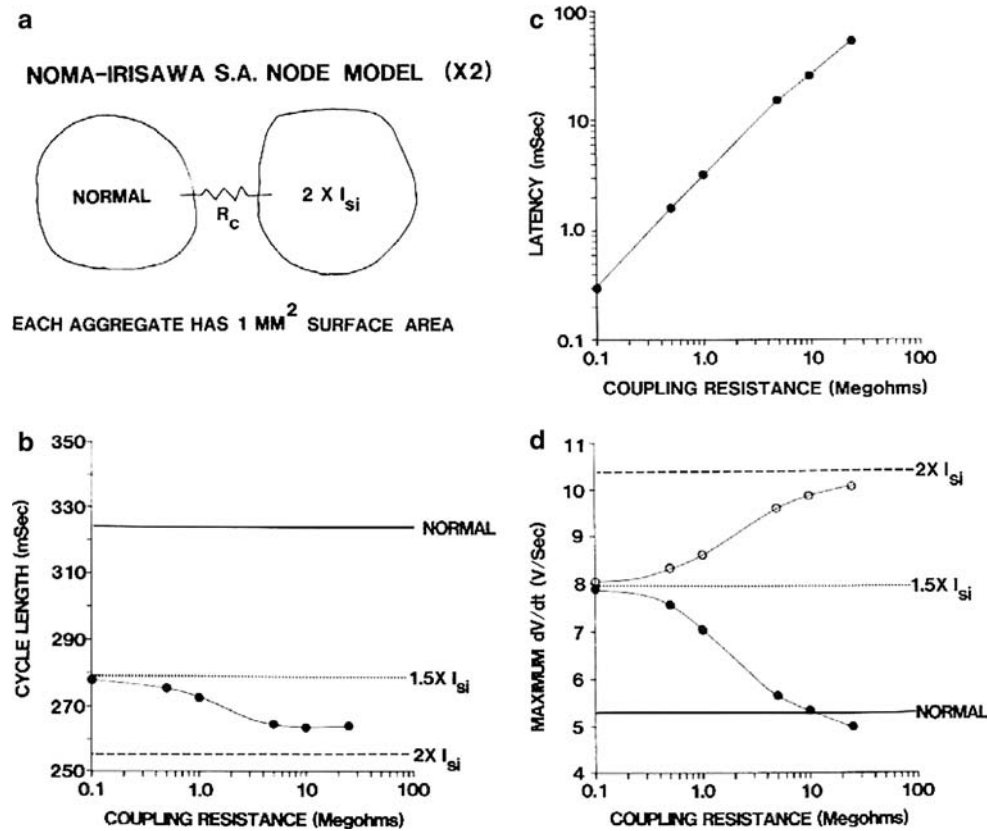


Fig. 1 Interactions between two coupled regions with intrinsically different pacing frequencies. **a** is a diagram of the simulation system for two isolated (groups of) cells with a coupling resistance R_c . **b** shows the relationship between coupling resistance and the entrained CL. The horizontal lines indicate the intrinsic CLs for isolated cells with the normal model (solid line) and the model with two times the normal L type Calcium current (I_{si}) (dashed line) and the model with 1.5 times the normal I_{si} (dotted line). **c** shows the latency between action

potentials occurring in the two groups of cells as a function of the coupling resistance. **d** shows the individual maximum dV/dt (V_{max}) values for the two groups of cells as functions of coupling resistance. The open circles are for the aggregate with the two times normal I_{si} model. The filled circles are for the aggregate with the normal model. As in (b), the horizontal lines indicate the intrinsic V_{max} for the models as labeled. From Joyner et al. [13]

action potentials. The effects of increased coupling resistance (e.g., fewer gap junctions) can be thought of as converting the process of consensual synchronization to that of local propagation in which the cells with greater intrinsic automaticity thus dominate the overall rate. Note also that the ability of the two aggregates to synchronize was preserved up to a coupling resistance of 25 M Ω , even though the surface area of the model aggregate (1×10^{-2} cm 2) was much larger than a single cell. From the approximate membrane surface area of only 20×10^{-6} cm 2 for single nodal cells, we could extrapolate from these results that a resistance of up to 12.5×10^9 Ω would allow synchronization of a pair of nodal cells. This corresponds to an intercellular coupling conductance of ~ 0.1 nS which could be produced by a very few gap junction channels.

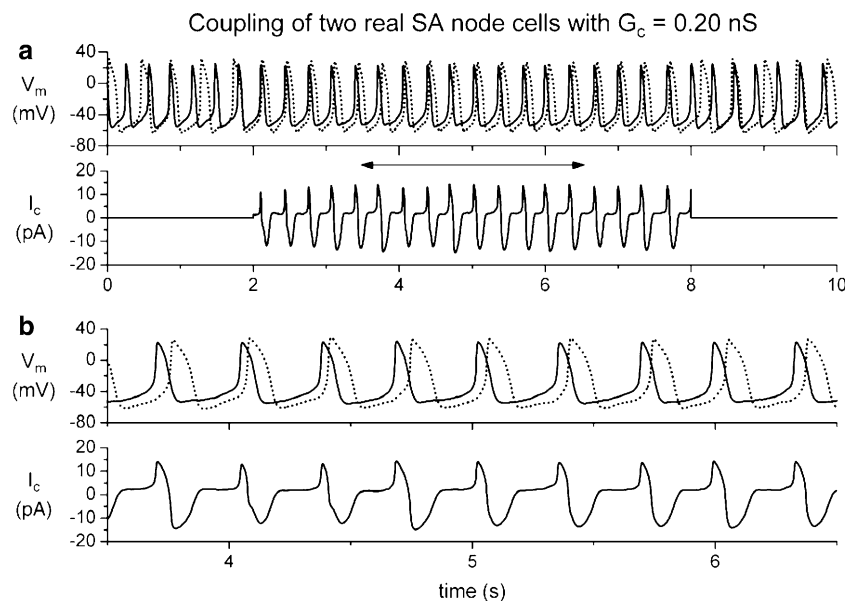
More recently, we used our “coupling clamp” circuit [24] to actually couple together isolated rabbit SA nodal cells with a defined coupling conductance [20]. In this technique, we simultaneously record the potential of two cells physically isolated from each other and use a computer system to calculate what coupling current would exist if there were a specified coupling conductance (G_c) and then, updated at short time intervals (e.g., 25 μ s), supply this time-varying current to one cell and the negative of this current to the other cell. Our results are shown in the top panel of Fig. 2a.

During the periods of uncoupling the spontaneous activity of cell A is occurring at a shorter interbeat interval (IBI) (310 ms) than the spontaneous activity of cell B (390 ms). The action potentials of the two cells are also somewhat different in shape, with cell A (*solid line*) having a less negative maximum diastolic poten-

tial (-57 mV vs. -62 mV) and a less positive peak amplitude (26 mV vs. 28 mV) than cell B (*dotted line*). Cell A also has a shorter action potential duration than cell B. The lower panel of Fig. 2a plots the coupling current for this cell pair. The coupling current is, of course, zero during the two periods of uncoupling, and is plotted as a positive current in the direction from cell A to cell B. When the cells are coupled even with this small coupling conductance ($G_c = 0.2$ nS) a stable pattern of entrainment of the action potentials of cell A and the action potentials of cell B is established during the period of coupling. In Fig. 2 the action potentials of cell A and cell B are entrained at a common IBI, but the shapes of the action potentials are still quite different for cell A and cell B, with cell B retaining a more negative maximum diastolic potential and a longer action potential duration. In other words, the cells show “frequency entrainment,” but not “waveform entrainment” [4]. When the coupling conductance was further increased to 10 nS (not shown) the action potentials of cell A and cell B are nearly synchronous during the period of coupling with the action potentials shapes now also nearly identical: the cells show both frequency and waveform entrainment.

If we define the successive activation times of either cell A or cell B as the times at which the membrane potential crosses zero in a positive direction, we can analyze the effects of the coupling conductance on the time-varying IBIs and the activation delays between cell A and cell B for coupled action potentials. Figure 3 illustrates the effects of coupling conductance of 0.2 nS for the same cell pair used for Fig. 2. The two cells show fluctuations of their IBI during the uncoupled

Fig. 2 Simultaneous recording for 10 s of two isolated rabbit sinoatrial node cells, with the cells uncoupled during the first 2 s and the last 2 s and coupled with a coupling conductance of 0.2 nS during the central 6 s. **a** Membrane potential (V_m ; upper panel) of cell A (*solid line*) and cell B (*dotted line*), and coupling current (I_c ; lower panel). **b** Data of part a replotted for the time period indicated by the horizontal two-headed arrow of **a**. From Verheijck et al. [20]



Interbeat interval and delay for two real SAN cells with 0.2 nS coupling

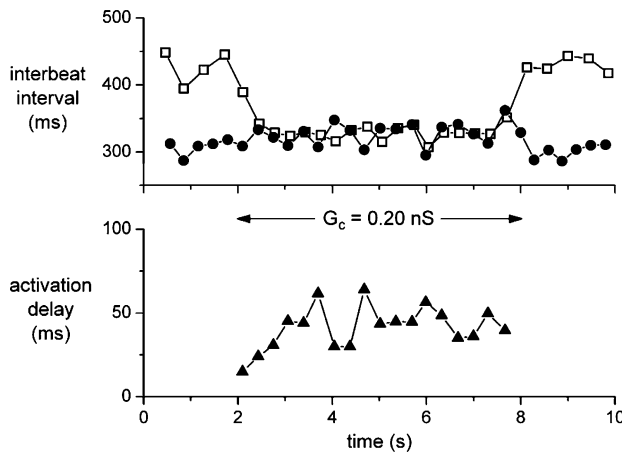


Fig. 3 Interbeat interval for the two rabbit SAN cells of Fig. 2 (upper panel; filled circles and open squares, respectively) and the delay in activation between the two cells (lower panel; filled triangles) for a coupling conductance $G_c = 0.2 \text{ nS}$ (indicated by a horizontal arrow). From Verheijck et al. [20]

periods, as previously demonstrated for isolated spontaneously active cells [22] with a coefficient of variation for IBI of about 4%, but during the coupling period the IBI of the two cells has a mean value slightly larger than that of the uncoupled IBI of cell A. Note that the common IBI is clearly not the arithmetic average of the IBI values for each of the cells. Fluctuations of IBI still occur during the coupling period with differences of up to 34 ms for IBI values of the two cells even for cycles, which are associated in time as part of the entrainment process. The activation delay (lower panel) shows significant fluctuations from 24 to 64 ms with an average value of 43 ms.

3 Interactions among a spontaneously pacing cell model and an atrial cell model

For the simulations shown in Fig. 1, we used two isotential spontaneously active membrane regions coupled by a resistance R_c . For the simulations of Fig. 4 we used an SA NODE region with the same Irisawa–Noma [10] model as for Fig. 1, and for the ATRIAL region we used the model of Beeler and Reuter [2] with the only modification being a reduction in the magnitude of the conductance for the slow inward current to 20% of the standard model to produce an action potential duration of $\sim 100 \text{ ms}$ to correspond with the atrial action potential duration [14]. It would have been more appropriate to also decrease the I_{K1} of the Beeler–Reuter model to match the input resistance of atrial cells (see section E) so these simulations

somewhat overestimate the effects of electrical load of the surrounding cells on the function of the SAN region. These results [14] illustrate the three possibilities of such a coupled system. Each symbol plotted represents a simulation of 2 s, with the simulation results being either (a) failure of the SA region to pace (NOT PACE, solid circle), (b) pacing of the SA region without activation of the atrial region (PACE BUT NOT DRIVE, open circle), or (c) pacing of the SA region with subsequent activation of the atrial region (PACE AND DRIVE, open triangle). We have not plotted symbols for all of the simulations performed, but only those, which delineate the boundaries between the defined regions on the graph. The solid line separates the graph space into regions of pacing and not pacing. The dashed line separates the graph space into regions of successful or unsuccessful driving of the atrial region. In part a, the membrane area of the atrial region is fixed at 1.0 mm^2 while the membrane area of the SA region and the coupling resistance are varied. Note that, for a fixed SA area of 1 mm^2 (same as for the ATRIAL area of this simulation) there is no value of coupling resistance, which allows successful PACE AND DRIVE. For larger values of SA area (e.g., 1.5 mm^2), the ability to PACE AND DRIVE is limited by the coupling resistance—too low coupling resistance and the SA region does not pace and too high coupling resistance and the SA region can pace but not drive the ATRIAL region. In part b, the membrane area of the SA region is fixed at 1.0 mm^2 while the membrane area of the atrial region and the coupling resistance are varied. The same phenomena are shown as for part a. Part c and d correspond to parts a and b, respectively, except that the magnitude of the slow inward current is doubled for the SA region in parts c and d. The major effect of this change in the properties of the SA region is that the parameter space which now allows successful PACE AND DRIVE is much larger. The boundary between PACE and NOT PACE is shifted to smaller SA area because the diastolic current is enhanced by increasing slow inward current. The boundary between PACE AND DRIVE and PACE BUT NOT DRIVE is also raised to higher values of coupling resistance because of the somewhat elevated peak amplitude of the SA region action potentials.

When we extended these simulations to a radial model of a distributed SAN-Atrial system, we were able to incorporate the differences in the gap junctional coupling among SAN cells as compared to atrial cells [18] with a radially distributed SAN system to investigate the effects of SAN size on the ability to propagate out from the SAN into the surrounding atrial tissue. We used a resistivity of $6,000 \Omega \text{ cm}$ within

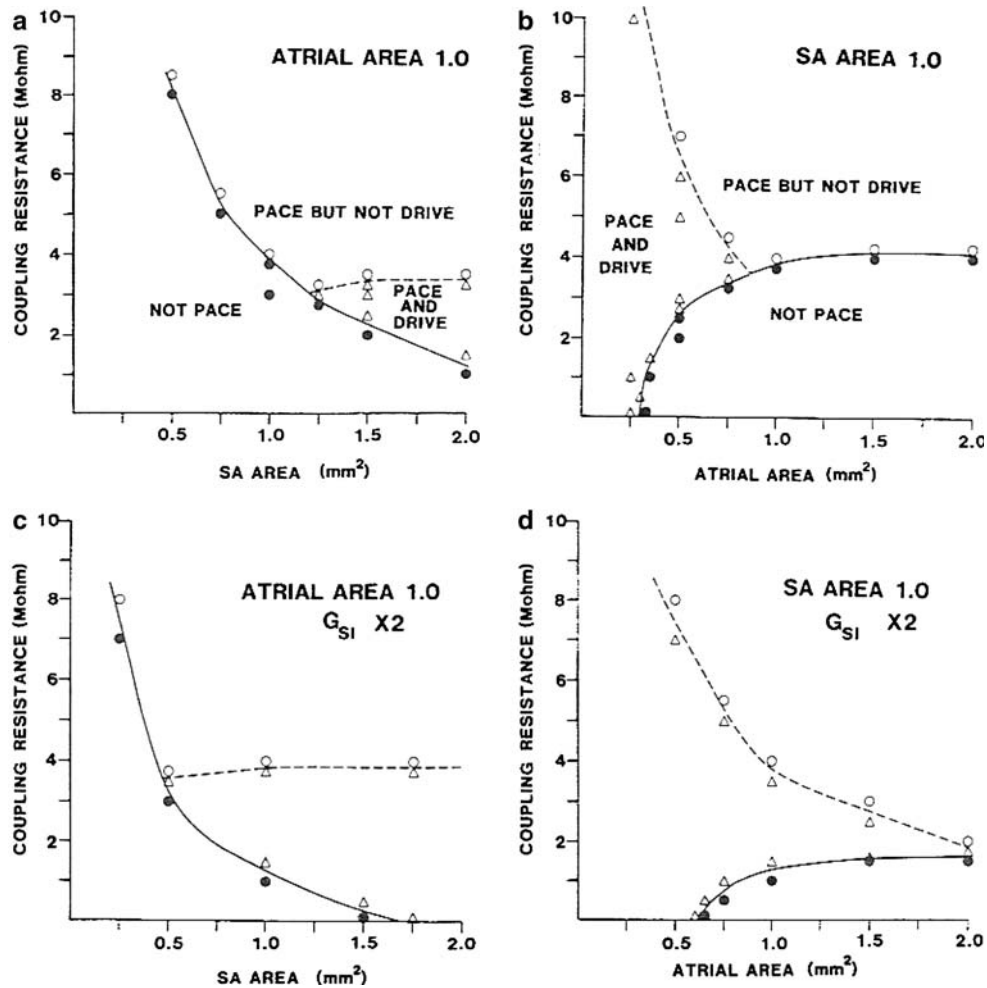


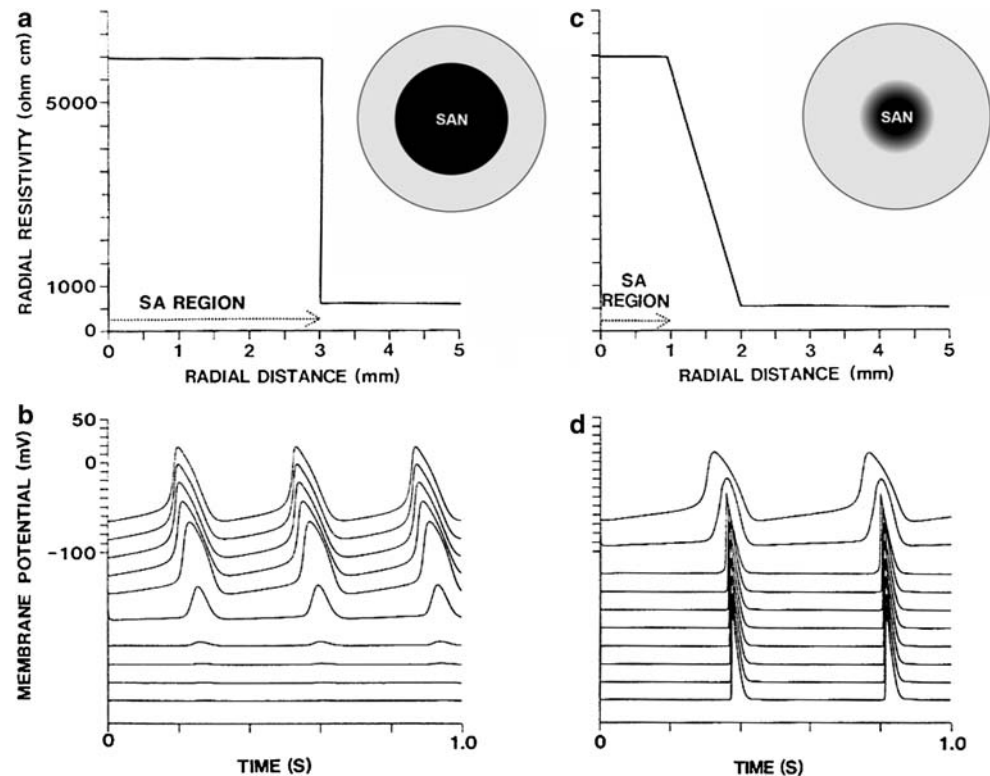
Fig. 4 Simulated results for two electrically coupled membrane regions (as in Fig. 1) for which the SA area is represented by the Irisawa–Noma [10] model and the atrial area is represented by a modified Beeler–Reuter [2] model with shortened action potential duration. Each symbol plotted represents a simulation of 2 s, with the simulation results being either (1) failure of the SA region to pace (NOT PACE, *solid circle*), (2) pacing of the SA region without activation of the atrial region (PACE BUT NOT DRIVE, *open circle*), or (3) pacing of the SA region with subsequent activation of the atrial region (PACE AND DRIVE, *open triangle*). In part **a**, the membrane area of the atrial region

is fixed at 1.0 mm² while the membrane area of the SA region and the coupling resistance are varied. In **b**, the membrane area of the SA region is fixed at 1.0 mm² while the membrane area of the atrial region and the coupling resistance are varied. The *solid line* separates the graph space into regions of pacing and not pacing. The *dashed line* separates the graph space into regions of successful or unsuccessful driving of the atrial region. **c** and **d** correspond to **a** and **b**, respectively, except that the magnitude of the slow inward current is doubled for the SA region in **c** and **d**. From Joyner et al. [14]

the SAN and only 600 Ω cm for the surrounding atrial tissue. This is depicted in the radial diagram in which high coupling resistance is shown as a dark area and low coupling resistance is shown as a gray area. However, we also varied the spatial abruptness with which the two regions merged. For the diagram of part **a**, we used an abrupt transition at a radial distance of 3 mm from the SAN membrane properties to the atrial membrane properties and the coupling resistance, as shown in the radial diagram and the plot of coupling resistance versus radial distance. For this radial model, the central SAN region paces at a high rate (being

electrically somewhat insulated by the high-coupling resistivity) but no propagation out into the surrounding atrial tissue occurs, even with an SAN radial distance of 3 mm (see part **b** of Fig. 5). This failure of propagation was strongly related to the increased electrical load as the action potential approached the SAN–Atrial boundary. When we made this boundary a more gradual transition, as shown in Fig. 5c, we got successful pacing of the SAN as well as propagation out into the atrial area even with an SAN radius of only 1 mm. Note that for the diagram of Fig. 5c and the simulation results of Fig. 5d, the concentric elements

Fig. 5 Results of two simulations with a radial disk model in which the radial resistivity within the SA node region is $6,000 \Omega \text{ cm}$. **a** and **c** are diagrams of two different radial distributions of radial resistivity and the SA node model in which diagram **a** has an abrupt decrease in radial resistivity and diagram **c** has a gradual decrease in radial resistivity into the surrounding atrial model cells. **b** and **d** are the simulation results for the distributions **a** and **c**, respectively, with **b** showing the SA node region continuing to PACE BUT NOT DRIVE while **d** shows slowing of the SA node rate but successful PACE AND DRIVE. From Joyner et al. [14]



with SAN membrane properties occur only within the central 1 mm and the coupling resistance is linearly decreased over the radial distance from 1 to 2 mm, as illustrated in the radial diagram. This suggests that a spatially inhomogeneous distribution of cell types and coupling resistance may be an essential feature of a successful SAN-Atrial interface.

4 Interactions among a spontaneously pacing cell model and a single quiescent real atrial cell

With our coupling clamp circuit, we were able to extend these simulations to couple together a model SAN cell, using the Wilders et al. [23] SAN cell model to real isolated rabbit atrial cells. The upper panel of Fig. 6a illustrates action potentials recorded from an isolated uncoupled rabbit atrial cell (solid line) paced by repetitive current pulses of 2 ms duration at a CL of 600 ms. The dashed line shows the steady state solution of membrane potential for the SAN model cell when the model cell is uncoupled ($G_C = 0$) from the real cell. We established coupling at a variety of conductance values to investigate the interactions between the two cells. The lower panel shows the membrane potential of the atrial cell (solid line) and the membrane potential of the SAN model cell (dashed line) for $G_C = 0.4 \text{ nS}$ and no stimuli applied to the atrial cell.

The coupled hybrid cell pair now has an increased CL of 437 ms (indicated by the horizontal arrow in the lower panel), with each AP produced in the SAN model cell accompanied, after a 52 ms delay (arrow), by a driven AP in the real atrial cell. We investigated the effects of a range of G_C for this hybrid cell pair, finding that for values $\geq 0.4 \text{ nS}$ there was propagation from the SAN model cell to this atrial cell with a decreasing conduction delay as G_C was increased. For $G_C < 0.3 \text{ nS}$ there was continued pacing of the SAN model without driving of the coupled atrial cell. For $0.3 < G_C < 0.4 \text{ nS}$ there was partial synchronization such that only some of the APs from the SAN model cell were conducted to the atrial cell. In Fig. 6b we show the same atrial cell with directly applied stimuli at CL 300 ms with $G_C = 0 \text{ nS}$ for the top panel and $G_C = 0.3 \text{ nS}$ in the lower panel. At this shorter CL, the directly paced atrial cell “overdrives” the SAN model cell with 1:1 conduction from the atrial cell to the SAN model cell.

However, when the directly paced CL of the atrial cell is longer than the intrinsic SAN model CL, arrhythmias may develop. Figure 6c shows results for the same real atrial cell as for Fig. 6a, b when we directly paced the real atrial cell at CL 600 ms and used $G_C = 0.4 \text{ nS}$. Under these conditions, if a spontaneous activation of the SAN model cell occurs when the real atrial cell is not refractory, propagation from the focus

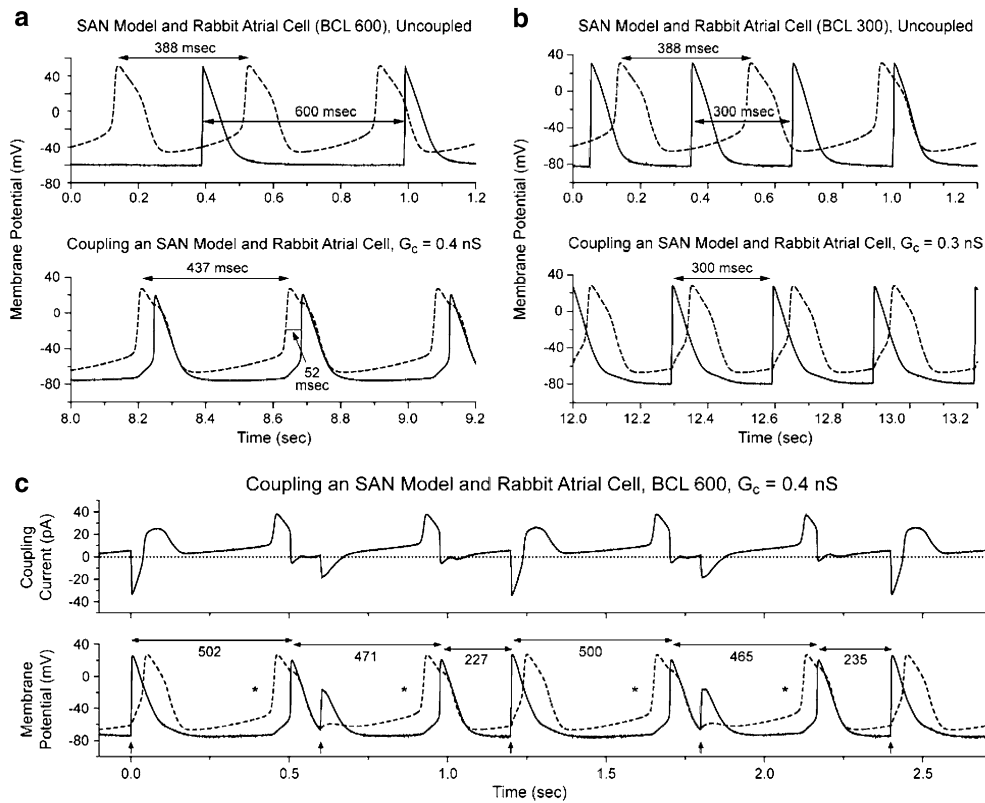


Fig. 6 Interactions between an SAN model cell [22] and a real rabbit atrial cell. **a** The upper panel shows action potentials recorded from an isolated uncoupled rabbit atrial cell (solid line) paced by repetitive current pulses of 2 ms duration at a basic cycle length (BCL) of 600 ms. The dashed line shows the steady state solution of membrane potential for the SAN model cell when the model cell is uncoupled ($G_c = 0$) from the real cell.

The lower panel shows the membrane potential of the atrial cell (solid line) and the membrane potential of the SAN model cell (dashed line) for $G_c = 0.4$ nS and no stimuli applied to the atrial cell. **b** The same atrial cell with directly applied stimuli at BCL 300 ms with $G_c = 0$ nS for the top panel and $G_c = 0.3$ nS in the lower panel. **c** Same real atrial cell paced at 600 ms with $G_c = 0.4$ nS coupling to the SAN model. From Joyner et al. [12]

model cell to the real atrial cell may occur. The data shown in Fig. 6c are from a longer recording after a steady-state condition had been established. The stimuli to the real atrial cell are shown as vertical arrows in the lower panel. The upper panel shows the coupling current, with a positive polarity indicating current flow from the SAN model cell to the real atrial cell. At time zero there is a stimulus, which directly activates the real atrial cell and this action potential propagates to the SAN model cell. The SAN model cell then has a spontaneous depolarization, which leads to an AP in the SAN model cell (indicated by an asterisk), which then propagates to the real atrial cell. The second direct stimulus to the real atrial cell (at time 0.6 s) now does not activate the real atrial cell because it is refractory. There is then another AP spontaneously generated in the SAN model cell (second asterisk), which also propagates to the real atrial cell. The third direct stimulus to the real atrial cell (at time 1.2 s) does activate the real atrial cell and this AP

propagates to the SAN model cell. This process then almost exactly repeats for the next three direct stimuli to the real atrial cell. The APs which occur in the real atrial cell are thus in an arrhythmic pattern, with a repeating series of 3 cycles (~500, 470, and 230 ms for an average CL of 400 ms) for each pair of direct stimuli at CL 600 ms. Note that in this simple two-cell system there is a bidirectional propagation, with the intrinsic automaticity of the focus cell being modulated by the propagation from the directly stimulated cell and also able to propagate to the quiescent cell.

5 Interactions between a focus region and surrounding two-dimensional tissue

We then used our coupling clamp system to couple together a real spontaneously active nodal cell (isolated from rabbit AV node) to a two-dimensional sheet of model cells, which would represent either atrial or

ventricular tissue by using specific models of each tissue type. Since we wanted to use arrays of model cells as surrogates for the electrical characteristics of two-dimensional arrays of either atrial or ventricular real cells, we tested the properties of the two models (for atrial cells [6], for ventricular cells [17]) as to their ability to re-create experimentally recorded differences in excitability of atrial and ventricular cells. For a stimulus frequency of 1 Hz, the atrial and ventricular cell models we used produce characteristically different action potential shapes, as expected. The ventricular cell model has a resting potential of -86 mV compared to -80 mV for the atrial cell model. The maximum dV/dt of the ventricular and atrial cell models are 379 and 220 V/s, respectively, with the amplitudes being 136 and 105 mV, respectively. These values are comparable to our previous experimental data [9] for the resting membrane potential, amplitude and maximum dV/dt measured from ten isolated rabbit atrial cells (-80 ± 1 mV, 109 ± 3 mV, and 206 ± 17 V/s, respectively) which differed significantly ($p < 0.05$) from those values we measured from six isolated rabbit ventricular cells (-82.7 ± 0.4 mV, 127 ± 1.12 mV, and 395 ± 21 V/s, respectively). Several fundamental differences in the membrane currents are included in these models. These differences include a lower value of maximum sodium conductance, lower value of the inward rectifier current (I_{K1}), and greater transient

outward current for the atrial model compared to the ventricular model and these differences are based on experimental data as described in the model papers.

For these studies, we isolated spontaneously active myocytes from the rabbit atrioventricular node region and then coupled a real nodal cell into a real-time simulation of a small sheet of cells with specified electrical coupling in the X and Y directions, as shown in Fig. 7a. From eight spontaneously active cells, the average CL when uncoupled was 340 ± 52 ms, with a maximum diastolic depolarization of -65 ± 8 mV, a peak positive amplitude of 36 ± 9 mV, and a maximum dV/dt of the rising phase of 13.6 ± 3.9 V/s. In the experimental protocol, we allowed the real nodal cell to automatically generate action potentials uncoupled from the sheet for the first 2 s of recording and then we coupled the sheet to the real nodal sheet for a further 10 s of recording. Figure 7b summarizes the results obtained by coupling the same nodal cells into either an atrial model sheet or a ventricular model sheet. The two variables that we used were the coupling conductance between cells of the sheet (G_X and G_Y) and also the “size” of the nodal cell. In order to change the effective “size” of the real cell, we scaled the current that was injected into the cell to accomplish the coupling to the sheet. Decreasing this current by a factor of two makes the nodal cell effectively two times larger. Generally, decreasing this current by a factor of Z

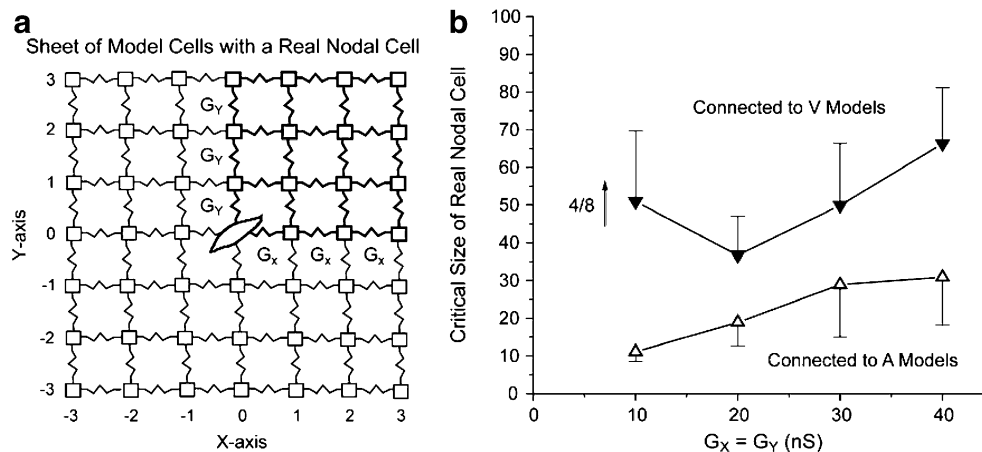


Fig. 7 **a** Diagram of the experimental setup in which a 7×7 array of cells is represented by a real central focus cell (isolated cell from the atrioventricular nodal area) is coupled to model elements which are real-time simulations of mathematical models of either ventricular or atrial cells (Luo and Rudy model [17] for ventricular cells, Courtemanche et al. model [6] for atrial cells). The coupling conductances (nS) in the X or Y directions are assumed to be constant and identical ($G_X = G_Y$). **b** Summary of results obtained from eight real isolated atrioventricular nodal cells by coupling each cell into atrial model arrays and

ventricular model arrays with coupling conductances of 10, 20, 30, or 40 nS and varying the size factor of the real nodal cell to determine the critical size which allows spontaneous activity of the nodal cell with propagation into each model array with each value of coupling conductance. For $G_X = G_Y = 10$ nS only 4 of the 8 nodal cells tested were able to successfully propagate into the V model array at any of the sizes (up to 100) tested. Data are shown as mean \pm SEM for the V model arrays (solid triangles) and the A model arrays (open triangles). From Joyner et al. [15]

makes the nodal cell effectively Z times larger, as if it consisted of a group of Z cells each well coupled to each other. Figure 7b shows that for a given value of $G_X = G_Y$, the critical size of the nodal region needs to be significantly larger for activation of a ventricular sheet than for an atrial sheet. In addition, the size of the nodal region is required to be larger when $G_X = G_Y$ is increased. Both of these effects can be explained by increases in the electrical load imposed by the sheet on the nodal cells. At the lowest value of $G_X = G_Y$ for the sheet, conduction into the atrial sheet continued but for the ventricular sheet 4 of the 8 cells had conduction block into the ventricular sheet.

6 Influences of two-dimensional tissue anisotropy and non-uniform anisotropy on the ability of a focus region to propagate

We also did experiments in which we coupled a real excitable cell into a two-dimensional sheet with anisotropy of the coupling conductances [21]. For these experiments we used a real guinea pig ventricular cell as a directly stimulated “focus” region to determine if propagation into a simulated sheet of ventricular model cells depended on the anisotropy of G_X and G_Y . The results are summarized in Fig. 8a. For this figure, the open symbols indicate failure of propagation into

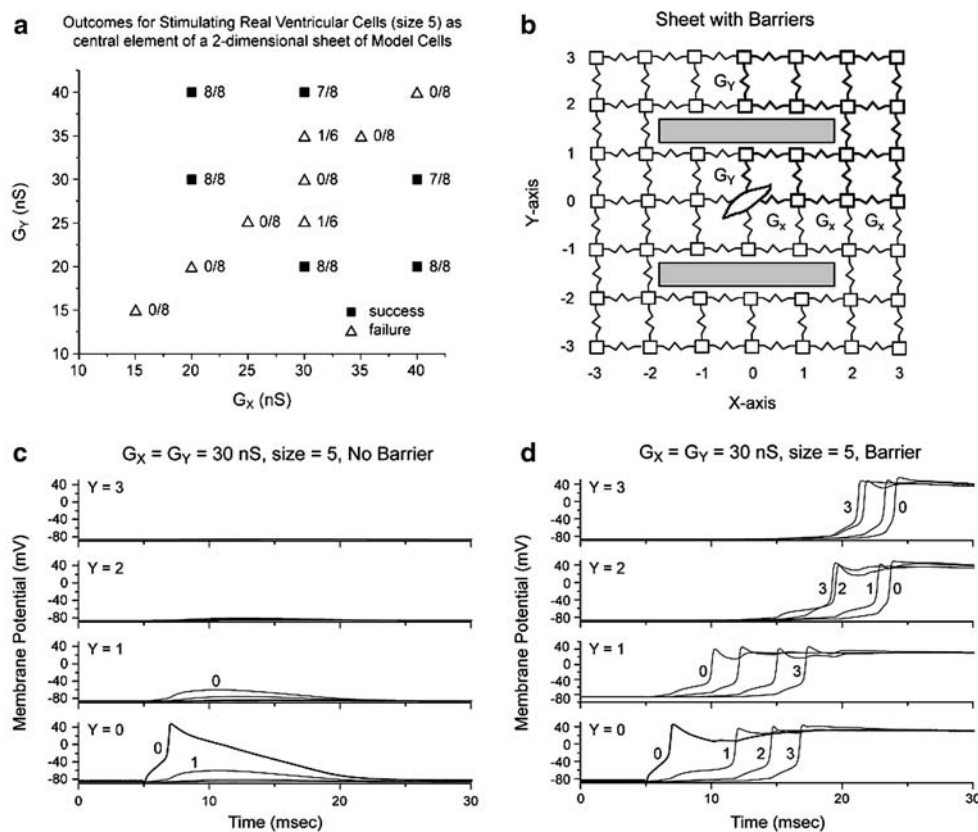


Fig. 8 **a** Diagram showing success or failure of propagation into the sheet for six real guinea pig ventricular cells as the central element of the sheet diagrammed in Fig. 7a. For each cell, using a size factor of five, we systematically varied G_X and G_Y to test the success or failure of propagation through the sheet when the real cell was repetitively stimulated at 1 Hz. The filled squares represent combinations of G_X and G_Y for which propagation was successful and the open symbols represent combinations of G_X and G_Y for which propagation failed. The fractions beside each symbol indicate the ratio of cells with successful propagations to the total number of cells tested with that combination of G_X and G_Y **b** Diagram of a two-dimensional sheet of excitable cells with resistive barriers. Each coupling conductance in the X direction has value G_X (nS) and each coupling conductance in the Y

direction has value G_Y (nS). The central element is represented by a real cell with a variable size and all other elements are represented by real-time simulations of the ventricular membrane model of Luo and Rudy [17] with the additional inclusion of two resistive barriers for which $G_Y = 0$ (gray bars). **c** Results for the stimulation of a real cell with size factor of five incorporated into the two-dimensional sheet of Fig. 7a (no barriers) with $G_X = G_Y = 30$ nS. The four panels show results for the four rows of elements ($Y = 0-3$) and within each panel the results for each of the four elements ($X = 0-3$) are labeled. The real cell has coordinates (0,0) and is plotted as a thicker line. **d** Results for the same cell and coupling conductances except for the inclusion of the resistive barriers, allowing successful propagation. From Wang et al. [21]

the sheet while the filled symbols indicate successful propagation into the sheet. For this example, with a size factor of five for the focus cell, propagation failed for $G_X = G_Y$ for values from 10 to 40 nS. However, when the sheet was made anisotropic (e.g., for $G_X = 30$ nS and G_Y either raised to 40 nS or lowered to 20 nS) propagation succeeded. The explanation is clearly not simply the total input resistance as seen from the focus region, but rather that, when the sheet is anisotropic, conduction occurs initially in the direction of the higher coupling conductance and this effectively raises the size of the focus region such that conduction can now occur in the direction of the lower coupling conductance.

A related phenomenon occurs when the sheet has non-uniform anisotropy, as exemplified in the diagram of Fig. 8b. In this scenario we incorporated resistive barriers representing connective tissue separations of cells such that the coupling resistance at that location is infinitively large. Figure 8c, d illustrates the results when the real cell is stimulated with $G_X = G_Y = 30$ nS with no resistive barriers and propagation fails into the sheet. For the same real cell, when we coupled this cell into the sheet with the resistive barriers, propagation succeeded parallel to the barriers and then progressed around the barriers to activate the entire sheet (Fig. 8d). Thus, the ability of a focus region to propagate out into surrounding tissue depends not only on the cell type of the tissue and the coupling conductances, but also the spatial distribution of the coupling conductances of the sheet. We also did simulations of propagation from a model SAN region into such spatially inhomogeneously coupled sheets and demonstrated these phenomena for a spontaneously active focus [25].

7 Summary

We have worked over several decades now on determining the design principles for successful propagation from a spontaneously active focus region to a surrounding syncytium of quiescent but excitable myocardium. These principles are of fundamental importance in the functioning of a normal SAN-Atrium interface as well as understanding how an abnormal focus can activate the entire heart. These principles can be briefly summarized as (1) central relative uncoupling to protect the spontaneously firing cells from too much electrotonic inhibition, (2) a transitional region in which the cell type and electrical coupling change from the central SAN region to the peripheral atrial region, and (3) a distributed

anisotropy to facilitate focal activity. There is increasing detail from three-dimensional reconstructions of how cell type and connexion type and density are distributed in such regions, such as the elegant studies of Dobrynski et al. [7]. Earlier work by Kodama and Boyett [16] demonstrated heterogeneity of action potential types in central versus peripheral regions of the SA node and more recent studies have demonstrated regional differences in gap junction type and distribution [5]. Anatomical studies of the rabbit SAN region show a very disorganized “mesh” of cells arranged around “islands” of connective tissue. There is also a spatially heterogeneous mixture of typical “central” SAN cells and “atrial” cells at the peripheral region of the SAN where these cell types can be distinguished by gap junction type as well as by several enzyme markers [7]. This anatomical structure and heterogeneity may provide the central uncoupling, the gradual transition, and the distributed anisotropy, which allows the SAN region to propagate into the atrial tissue. Recent work by Benson et al. [3] demonstrating a specific sodium channel mutation related to sick sinus syndrome in humans may also indicate clinical significance of loading effects on human SAN atrial conduction. The bidirectional effects at the SAN-Atrial interface or at the interface between an ectopic focus in the atrium or the ventricle continue to be of considerable research interest and clinical significance.

References

1. Auricchio A, Klein H (2000) Arrhythmias in heart failure. *Curr Treat Options Cardiovasc Med* 2(4):329–339
2. Beeler GW, Reuter H (1977) Reconstruction of the action potential of ventricular myocardial fibres. *J Physiol* 268:177–210
3. Benson DW, Wang DW, Dymment M, Knilans TK, Fish FA, Strieper MJ, Rhodes TH, George AL Jr (2003) Congenital sick sinus syndrome caused by recessive mutations in the cardiac sodium channel gene (SCN5A). *J Clin Invest* 112(7):1019–1028
4. Cai D, Winslow RL, Noble D (1994) Effects of gap junction conductance on dynamics of sinoatrial node cells: two-cell and large-scale network models. *IEEE Trans Biomed Eng* 41(3):217–231
5. Coppen SR, Kodama I, Boyett MR, Dobrzynski H, Takagishi Y, Honjo H, Yeh HI, Severs NJ (1999) Connexion45, a major connexion of the rabbit sinoatrial node, is co-expressed with connexion43 in a restricted zone at the nodal-crista terminalis border. *J Histochem Cytochem* 47(7):907–918
6. Courtemanche M, Ramirez RJ, Nattel S (1998) Ionic mechanisms underlying human atrial action potential properties: insights from a mathematical model. *Am J Physiol* 275(1 Pt 2):H301–H321

7. Dobrzynski H, Li J, Tellez J, Greener ID, Nikolski VP, Wright SE, Parson SH, Jones SA, Lancaster MK, Yamamoto M, Honjo H, Takagishi Y, Kodama I, Efimov IR, Billeter R, Boyett MR (2005) Computer three-dimensional reconstruction of the sinoatrial node. *Circulation* 111(7):846–854
8. Efimov IR, Nikolski VP, Rothenberg F, Greener ID, Li J, Dobrzynski H, Boyett M (2004) Structure-function relationship in the AV junction. *Anat Rec A Discov Mol Cell Evol Biol* 280(2):952–965
9. Golod DA, Kumar R, Joyner RW (1998) Determinants of action potential initiation in isolated rabbit atrial and ventricular myocytes. *Am J Physiol* 274:H1902–H1913
10. Irisawa H, Noma A (1982) Pacemaker mechanisms of rabbit sinoatrial node cells. In: Bouman HN, Jongsma HJ (eds) *Cardiac rate and rhythm*. Martinus Nijhoff Publishers, The Hague, pp 35–52
11. Janse MJ, Opthof T, Kleber AG (1998) Animal models of cardiac arrhythmias. (review) (163 refs). *Cardiovasc Res* 39(1):165–177
12. Joyner RW, Kumar R, Golod DA, Wilders R, Jongsma HJ, Verheijck EE, Bouman L, Goolsby WN, van Ginneken AC (1998) Electrical interactions between a rabbit atrial cell and a nodal cell model. *Am J Physiol* 274(6 Pt 2):H2152–H2162
13. Joyner RW, Picone J, Veenstra R, Rawling D (1983) Propagation through electrically coupled cells. Effects of regional changes in membrane properties. *Circ Res* 53(4):526–534
14. Joyner RW, van Capelle FJL (1986) Propagation through electrically coupled cells: how a small SA node drives a large atrium? *Biophys J* 50:1157–1164
15. Joyner RW, Wang YG, Wilders R, Golod DA, Wagner MB, Kumar R, Goolsby WN (2000) A spontaneously active focus drives a model atrial sheet more easily than a model ventricular sheet. *Am J Physiol Heart Circ Physiol* 279(2):H752–H763
16. Kodama I, Boyett MR (1985) Regional differences in the electrical activity of the rabbit sinus node. *Pflugers Arch* 404:214–226
17. Luo CH, Rudy Y (1994) A dynamic model of the cardiac ventricular action potential. I. Simulations of ionic currents and concentration changes. *Circ Res* 74:1071–1096
18. Masson-Pevet MA, Bleeker WK, Besselsen E, Mackaay AJC, Jongsma HJ, Bouman LN (1982) On the ultrastructural identification of pacemaker cell types. In: Bouman LN, Jongsma HJ (eds) *Cardiac rate and rhythm*. Martinus Nijhoff, The Hague, pp19–34
19. Veenstra RD, DeHaan RL (1986) Electrotonic interactions between aggregates of chick embryo cardiac pacemaker cells. *Am J Physiol* 250:H453–H463
20. Verheijck EE, Wilders R, Joyner RW, Golod DA, Kumar R, Jongsma HJ, Bouman LN, van Ginneken AC (1998) Pacemaker synchronization of electrically coupled rabbit sinoatrial node cells. *J Gen Physiol* 111:95–112
21. Wang YG, Kumar R, Wagner MB, Wilders R, Golod DA, Goolsby WN, Joyner RW (2000) Electrical interactions between a real ventricular cell and an anisotropic two-dimensional sheet of model cells. *Am J Physiol Heart Circ Physiol* 278(2):H452–H460
22. Wilders R, Jongsma HJ (1993) Beating irregularity of single pacemaker cells isolated from the rabbit sinoatrial node. *Biophys J* 65:2601–2613
23. Wilders R, Jongsma HJ, van Ginneken AC (1991) Pacemaker activity of the rabbit sinoatrial node. A comparison of mathematical models. *Biophys J* 60:1202–1216
24. Wilders R, Kumar R, Joyner RW, Jongsma HJ, Verheijck EE, Golod D, van Ginneken AC, Goolsby WN (1996) Action potential conduction between a ventricular cell model and an isolated ventricular cell. *Biophys J* 70(1):281–295
25. Wilders R, Wagner MB, Golod DA, Kumar R, Wang YG, Goolsby WN, Joyner RW, Jongsma HJ (2000) Effects of anisotropy on the development of cardiac arrhythmias associated with focal activity. *Pflugers Arch* 441(2–3):301–312